17th World Conference on Earthquake Engineering, 17WCEE
Sendai, Japan - September 13th to 18th 2020

PRELIMINARY STUDY OF CURVED-BASE POST-TENSIONED ROCKING WALLS

R. Wiebe[(1)], C.-P. Lin[(2)], J. W. Berman[(3)]

[(1)] *Assistant Professor, University of Washington, rwiebe@uw.edu*
[(2)] *Graduate Research Assistant, University of Washington, cpl7@uw.edu*
[(3)] *Professor, University of Washington, jwberman@uw.edu*

Abstract

Post-tensioned rocking walls coupled with energy dissipation devices have gained attention, as they are able to achieve little to no residual drift and simplify repairs after extreme events. However, several additional challenges remain. Traditional walls are susceptible to base compression damage and yielding in the post-tensioned bars; the latter is critical, as post-tensioned bars provide re-centering and lateral resistance to the system. The work here presents the concept of curved-base rocking walls, a modification to traditional rectangular profile walls. This geometric modification offers a solution for the challenges mentioned and offers additional potential benefits, which are explored in this work. The static and dynamic behavior of curved-base rocking walls coupled with gravity frames are studied with analytical equations. These equations also provide further insight into the parameter sensitivities and identify key components that drive the behavior. A finite element model is also used to validate the analytical results. Furthermore, a preliminary investigation of how curved-base rocking walls may improve performance and how the modifications effect the static and dynamic response is presented. Finally, a discussion on performance-based design of rocking walls (including curved-base rocking walls) is also included.

Keywords: rocking wall; precast wall; CLT wall; earthquake engineering; curved base

1. Introduction

Research on the socio-economic effects of earthquakes has motivated interest in developing lateral resistance systems that can improve the seismic resilience of buildings. Recent developments in lateral force resisting systems have focused on designing the structure to remain operational and require minimal repair after an earthquake. This objective will likely require that the primary structure remain elastic (i.e., undamaged) and a secondary system to provide supplementary energy dissipation. Rocking lateral-force resisting systems using post-tensioned (PT) rocking walls, have been shown to meet this objective.

There are some challenges in rocking walls that still needs to be addressed: first, the risk of compression base damage from stress concentration when rocking on the toe, i.e., toe crushing; and second, yielding (and/or fracturing) of the PT bars. The work here presents the concept of PT curved-base rocking walls (CBRWs) as a solution to these challenges and also to provide additional design parameters for engineers to optimize lateral resistance systems. The results of the work presented herein, using analytical equations and finite element (FE) analysis, strive to provide fundamental and practical knowledge to aid in the advancement of rocking systems in the field of earthquake engineering.

1.1 Review of free-standing rigid blocks

Using the principle of conservation of angular momentum, Housner was able to find the energy dissipated from base-ground impact for a single-joint rocking block and applied it to the equation of motion to develop the Simple Rocking Model (SRM) [1]. Work by others has greatly contributed to the understanding of free-standing rocking block behavior [1-6]. Good insight into the response of rocking blocks through closed-form equations have been provided by analytical work; however, they are mostly limited to free vibration and pulse loading due to the complex nonlinear and non-smooth behavior of rocking systems. For forced response, numerical studies have shown rocking systems are tremendously sensitive to system parameters and initial conditions [7, 8]. In order to improve stability, Bachmann et al. looked at free-standing rigid columns with curved base of constant curvature [9], which is relevant to the work herein.

1.2 Review of post-tensioned rocking systems for seismic applications

The combination of the rocking mechanism, PT bars, and energy dissipation devices results in a ‘flag-shaped’ hysteresis curve [10, 11]. This provides re-centering and limits peak drifts. The robust seismic performance of PT rocking structures coupled with energy dissipation devices have been demonstrated in [12, 13]. The Lagrange equation was used to formulate the equation of motion for rocking frames [14]. Studies have shown that the static and dynamic behavior of the system are largely effected by the contact stiffness between the rocking structure and the contact surface [15, 16].

A large-scale five-story structure with precast concrete connections and rocking walls was tested by the Precast Seismic Structural Systems (PRESSS) project [12, 17]. The project resulted in design and detailing requirements in ACI 318-14. Henry et al. looked at concrete crushing at the toe of the precast rocking walls [18]. Studies on timber rocking walls using cross-laminated timber (CLT) and laminated veneer lumber (LVL) have been conducted recently [19, 20, 13, 21-23]. Eatherton et al. investigated and compared rocking steel-braced frames with other conventional and self-centering seismic force resisting systems [24].

2. Curved-base rocking walls and formulation of analytical equations

2.1 Impetus for curved-base rocking walls

As mentioned above, there are challenges for rocking systems that still persist. The work presented here explores the concept of a curved-base rocking wall (CBRW) — see Fig. 1 — that address the challenges, and increase control over seismic performance and resilience of rocking wall structures. By using a curved base, several advantages are introduced: (1) the stress concentration on the corner of the wall is decreased. (2) The geometry of the CBRW provides confinement for the material at the contact surface, which may be especially important for reinforced concrete walls. (3) The geometry of the curved base also allows the wall to drift further before the PT bars start to yield (i.e., increase drift yield capacity) due to the decrease in height as the

© The 17th World Conference on Earthquake Engineering

wall rolls on the curved surface. (4) The force-displacement response can be tailored with multiple effective stiffnesses.

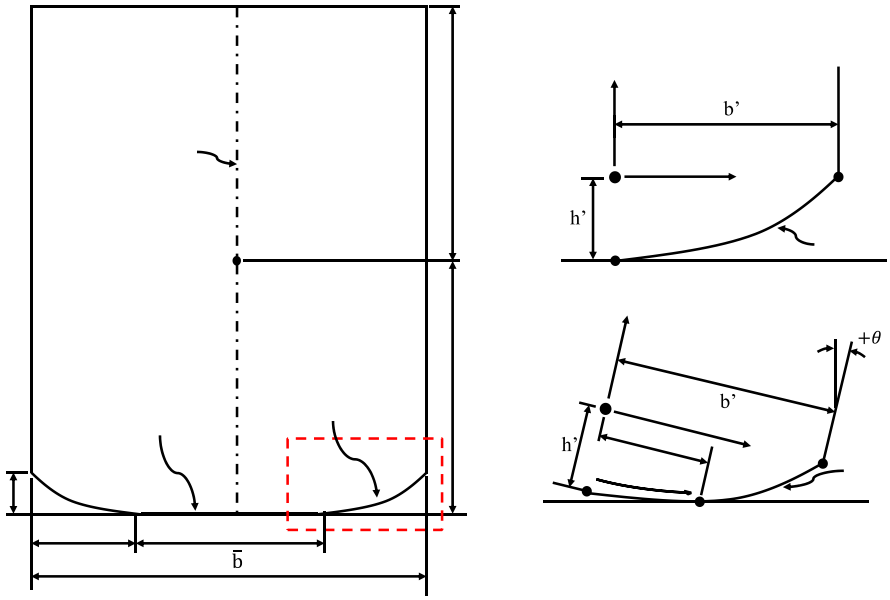

Fig. 1 – Diagram of a curved-base rocking wall

2.2 Curved-base rocking wall modeling assumptions

Energy dissipation devices were omitted, and the rocking walls and gravity frame were idealized as rigid elements in order to study the properties specific to the CBRW. It is assumed that no sliding or jumping occurs. The mass of the wall and floors were lumped at their respective centers of mass (see Fig. 2). This was done to enable the comparison with a lumped mass FE model that will be discussed later. The PT bars were modeled as perfectly elastic (in practice, the PT bars are designed in order to remain elastic under expected drift demands). All models herein checked the strains of the PT bars throughout the simulations to be below the yield strain of typical PT bars (0.0032).

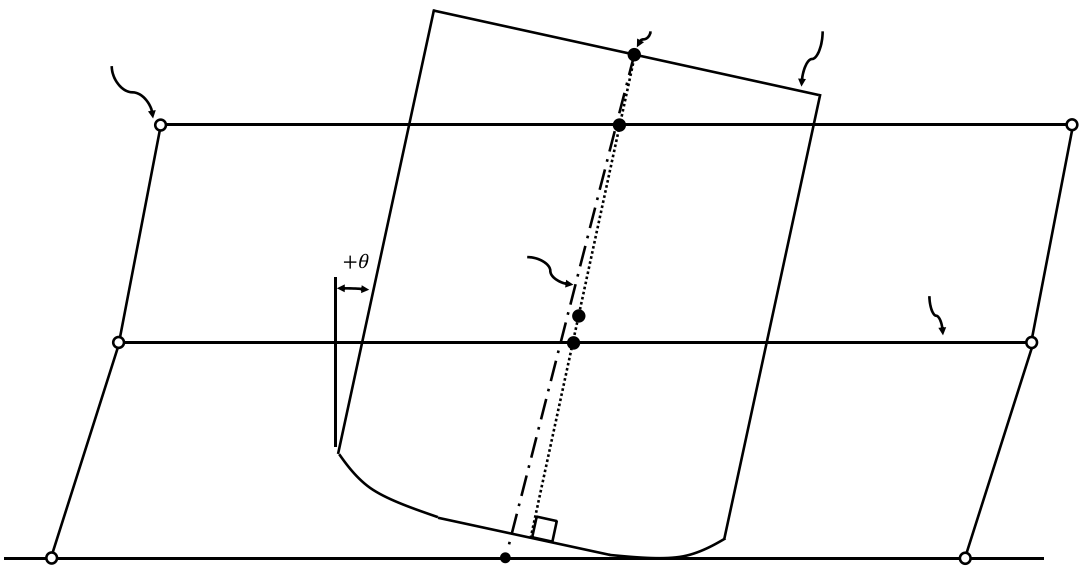

Fig. 2 – Model of rocking wall and gravity frame

© The 17th World Conference on Earthquake Engineering

2.3 Kinematics

2.3.1 Kinematics of rocking wall

The formulation of the analytical equations requires the kinematic relationships between the position of the wall and a generalized coordinate. The generalized coordinate used herein is the wall rotation angle — i.e., tilt angle (θ). There are three different rocking stages: (1) rocking about the inner corner; (2) rolling on the curved surface; and (3) rocking about the outer corner. A wide range of functions may be suitable for the curved portion of the base; however, an exponential function was used. An exponential function was chosen because it is integrable and it allows for somewhat independent control of the height, width, and sharpness of the curved section via three parameters h′, b′, and α, respectively. The curve is given by Eq. (1), where β is a dependent variable given by Eq. (2), and x and y are local coordinates (see Fig. 1).

$$y = \beta(e^{\alpha x} - 1) - h' \tag{1}$$

$$\beta = \frac{h'}{e^{\alpha b'} - 1} \tag{2}$$

The displaced horizontal and vertical positions of the PT bars attachment point on the wall, u_{PT} and v_{PT}, are obtained from the following equations (only equations for stage 2 is shown):

$$u_{PT} = R_{PT}\sin(\theta - \phi_{PT}) + \frac{\bar{b}}{2} + \text{arc length}(x) - x(\theta)\cos(\theta) - y(\theta)\sin(\theta) \tag{3a}$$

$$v_{PT} = R_{PT}\cos(\theta - \phi_{PT}) + x(\theta)\sin(\theta) - y(\theta)\cos(\theta) \tag{3b}$$

$$R_{PT} = \sqrt{\left(\frac{\bar{b}}{2}\right)^2 + (2h_w - h')^2} \tag{3c}$$

$$\phi_{PT} = \arctan\left(\frac{\bar{b}/2}{2h_w - h'}\right) \tag{3d}$$

Any other displaced position of the wall, e.g., center of mass of the wall, is similarly calculated since the wall is rigid.

2.3.2 Kinematics of gravity frame

The gravity frame exerts a seismic inertial lateral force through special diaphragm connections [12, 25, 26]. For the gravity frame to wall connections used herein (see Fig. 3), the following kinematic relations between θ and the displaced position of the floors, u_i and v_i, were derived for a two-story frame, where i denotes the floor number (only the kinematic equations from first floor are shown):

$$\tan(\theta) = \frac{\bar{u}_1 - u_1}{\bar{v}_1 - v_1} \tag{4a}$$

$$v_1 = \sqrt{h_1^2 - u_1^2} \tag{4b}$$

where $\bar{u}_1$ and $\bar{v}_1$ are the horizontal and vertical displaced position of the initial connection points (i.e., the contact point on the wall when the structure is plumb).

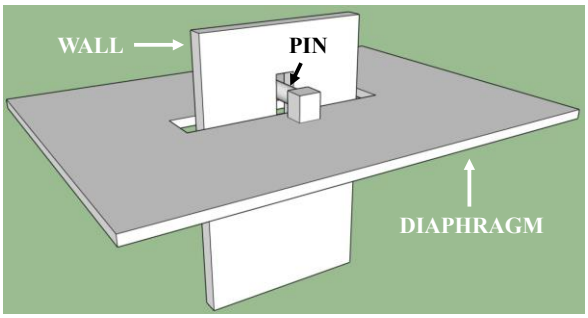

Fig. 3 – Diagram of wall-to-diaphragm connection

© The 17th World Conference on Earthquake Engineering

2.4 Formulation of governing equation

The Lagrange equation is used to derive the governing equation (i.e., equation of motion),

$$\frac{d}{dt}\left(\frac{\partial T}{\partial \dot{\theta}}\right) - \frac{\partial T}{\partial \theta} + \frac{\partial V}{\partial \theta} = 0 \tag{5}$$

where T and V are the kinetic and potential energy, respectively, and the time derivative is represented by a dot above the variable. Equations (6), (7), and (8) provide the expanded terms in Eq. (5):

$$\frac{\partial V}{\partial \theta} = k\Delta\frac{\partial \Delta}{\partial \Delta} + g\left(m_w\frac{\partial v_w}{\partial \theta} + \sum_{i=1}^{n} m_i\frac{\partial v_i}{\partial \theta}\right) \tag{6}$$

where n, k, Δ, and g are the number of floors, PT bars stiffness, PT bar elongation (measured from the zero stress state), and acceleration due to gravity, respectively. m_w and m_i denote the mass of the wall and floors, respectively. Note that the terms with m_i is the overturning P-Δ effects. After differentiating T, and some manipulation and combination, and by separating u into the relative and ground motion terms ($u \rightarrow u + u_g$):

$$\frac{d}{dt}\left(\frac{\partial T}{\partial \dot{\theta}}\right) - \frac{\partial T}{\partial \theta} = I_{dyn}(\theta)\ddot{\theta} + G(\theta)\dot{\theta}^2 + M_g(t,\theta) = 0 \tag{7}$$

where,

$$I_{dyn}(\theta) = m_w\left[\left(\frac{\partial u_w}{\partial \theta}\right)^2 + \left(\frac{\partial v_w}{\partial \theta}\right)^2\right] + \sum_{i=1}^{n} m_i\left[\left(\frac{\partial u_i}{\partial \theta}\right)^2 + \left(\frac{\partial v_i}{\partial \theta}\right)^2\right] \tag{8a}$$

$$G(\theta) = m_w\left[\left(\frac{\partial^2 u_w}{\partial \theta^2}\right)\frac{\partial u_w}{\partial \theta} + \left(\frac{\partial^2 v_w}{\partial \theta^2}\right)\frac{\partial v_w}{\partial \theta}\right] + \sum_{i=1}^{n} m_i\left[\left(\frac{\partial^2 u_i}{\partial \theta^2}\right)\frac{\partial u_i}{\partial \theta} + \left(\frac{\partial^2 v_i}{\partial \theta^2}\right)\frac{\partial v_i}{\partial \theta}\right] \tag{8b}$$

$$M_g(t,\theta) = \left(m_w\frac{\partial u_w}{\partial \theta}\right)\ddot{u}_g + \sum_{i=1}^{n}\left(m_i\frac{\partial u_i}{\partial \theta}\right)\ddot{u}_g \tag{8c}$$

3. Verification of analytical equations with finite element model

The design of the rocking system was based on a CLT rocking wall shake table test [26], with the following modifications: (1) curving the base, (2) modeling only one panel of one of the coupled rocking, (3) removing the UFPs, (4) relocating the PT bars to a single concentric location. The values for key parameters are provided in Table 1, where A_{PT}, T_o, and E_{PT} are the total area, total initial force, and modulus of elasticity of the PT bar, respectively. Note that the values of the parameters for the curved base provided in the next two sections were chosen to show the differences between the pushover backbone of a CBRW and a rectangular wall, and to induce more stage 2 rocking. A concentrated lateral force was applied at the PT bars attachment point at the top of the wall for the pushover analyses.

Table 1 – Rocking wall baseline design

h_w (in)	h_1 (in)	h_2 (in)	b (in)	m_w (kip/in/s^2)	m_1 (kip/in/s^2)	m_2 (kip/in/s^2)	A_{PT} (in^2)	T_o (kip)	E_{PT} (ksi)
144	146	120	60	0.0055	0.0594	0.0612	1.7668	48	29000

Very stiff beam-column elements were used to model the wall, beams and columns of the gravity frame in OpenSees [27]. Similarly, stiff shear springs were connected from the base of the wall to the ground via truss elements to prevent sliding. The diaphragms were connected to the wall by vertical beam-column elements with a large bending stiffness and low axial stiffness. The curved base was modeled with rigid zero-length compression-only springs with gap parameters. A diagram of the FE model, the zero-length compression-only springs, and the force-deformation plot of the compression-only spring is shown in Fig. 4.

3.1 Comparison of analytical and finite element model

Figure 5 (left) shows the pushover results (normalized by the decompression moment, M_{dec}) of the CBRW and the rectangular wall. M_{dec} is 125.38 kip-ft. and 25.08 kip-ft. for the rectangular wall and CBRW,

© The 17th World Conference on Earthquake Engineering

respectively. The model uses the same parameters in Table 1 with additional curved base parameters seen in Fig. 5. The pushover analyses show that the potential energy terms and the kinematic equations match with the FE model. Also, Fig. 5 (left) shows the drift is zero until the joint opens, which is the case when the structure and contact surface is assumed to be rigid.

For the nonlinear time-history analysis, impact damping was neglected here in order to isolate the effects of the governing equations derived in the previous section. Undamped free vibration simulations were performed, thus, the simulation captured, in effect, the natural frequency of the CBRW. Figure 5 (right) shows a plot of θ versus time from the analytical equations and the FE model. It is evident that all equations and the FE model agree.

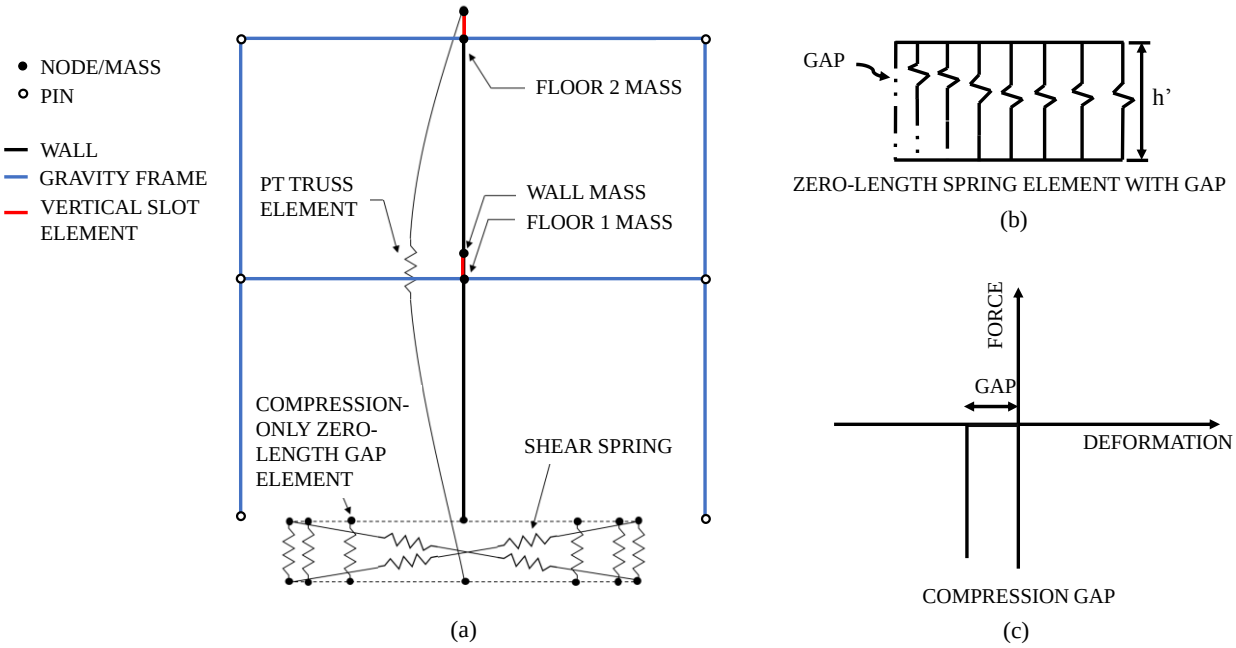

Fig. 4 – (a) Diagram of finite element model, (b) schematic of compression-only zero-length gap element, (c) plot of force-deformation response of compression-only zero-length gap element

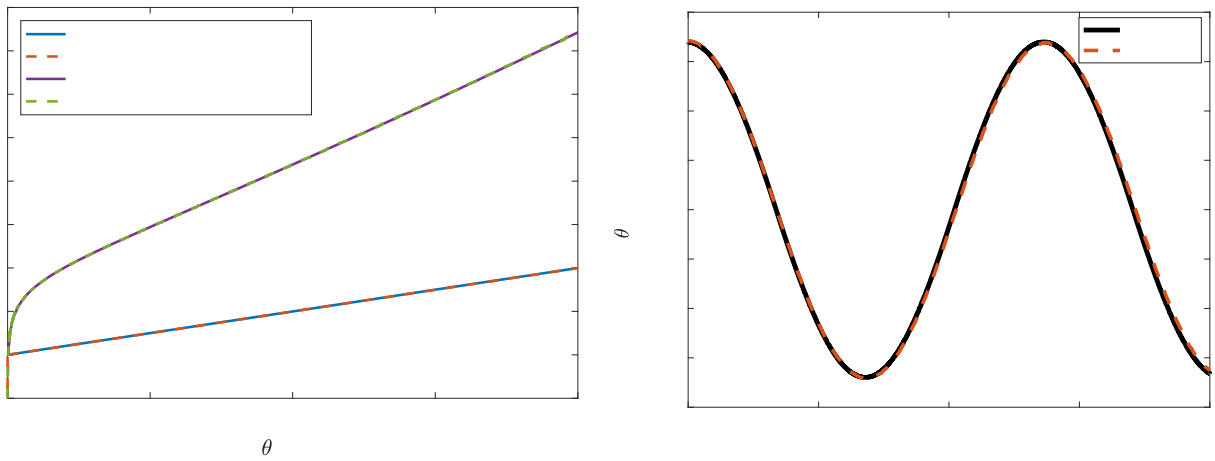

Fig. 5 – Comparison between analytical and finite element model: pushover response (left), nonlinear time-history analysis (right)

© The 17th World Conference on Earthquake Engineering

4. Effects of curved-base rocking walls

4.1 Increase of elastic capacity

Several curved base (and rectangular) configurations were used to look at the interactions between the curved base parameters. Table 2 includes the design values for the different CBRWs (the design for rectangular walls can similarly be obtain from columns 1 to 3 of Table 2) with remaining design values given in Table 1. The design values were chosen to increase in δ_y with a constant M_{dec}. The baseline design (see Table 1) is denoted herein with the subscript o.

Figure 6 shows the pushover backbone curve up to the onset of PT bar yielding. Note that capacity in Fig. 6 refers to the normalized restoring moment and θ at the onset of PT bar yielding. Figure 6 shows an increase in δ_y for the CBRWs and with the same backbone curve of the baseline rectangular wall. This is without a rigorous optimization routine. In addition, Fig. 6 (bottom) shows an almost linear relationship between A_{PT}/A_{PTo} and δ_y/δ_{yo} with the condition that M_{dec} and post-decompression stiffness are to remain constant. The relationship between A_{PT}/A_{PTo} and δ_y/δ_{yo} is a highly complex implicit relationship but is nearly linear despite the nonlinearities in CBRWs.

Table 2 – Curved-base rocking wall design

Design	A_{PT}/A_{PTo}	$\bar{b}$ (in)	b' (in)	h' (in)	α (1/in)	θ_{1-2} (rad)	θ_{1-2} (rad)
CBRW 1	1.10	55	2.50	0.30	2.50	1.45 E-3	0.64
CBRW 2	1.15	52	4.00	1.75	2.50	1.99 E-3	1.35
CBRW 3	1.20	50.4	4.80	2.00	1.80	6.37 E-3	1.30
CBRW 4	1.25	48.4	5.80	2.00	1.50	5.00 E-3	1.25
CBRW 5	1.50	40.64	9.68	5.00	0.90	7.41 E-3	1.35
CBRW 6	2.00	30.72	14.64	10.00	0.59	1.05 E-3	1.40
CBRW 7	2.50	24.70	17.65	12.00	0.47	1.41 E-3	1.40

4.2 Tailoring multiple stiffnesses

Figure 7 demonstrates how CBRWs fit in between a narrow and wide wall. The $M_{restoring}$ reduction from line 1 and line 3 is caused by the horizontal translation and height decrease when transitioning from stage 1 to stage 3 rocking. Note, the post-tensioning remained constant for all four wall geometries. Figure 7 also illustrates qualitatively how the CBRW can be tailored to respond as both a wide and narrow rectangular wall due to the multiple-rocking stage response. One of the main advantage of CBRWs is the multiple stiffness from the different rocking stages (see Wall 2 in Fig. 7). The pushover response can be modified to different performance objectives for different hazard levels. Although not visible in Fig. 7, the tailorability of the pushover response also suggests the possibility of tuning multiple natural periods of the rocking system for devices such as tuned mass dampers.

4.3 Gyroscopic effect

The governing equation formulated for CBRWs in Sec. 2.4 – see Eq. (8c) – contains a gyroscopic term not present in rectangular walls. Undamped free vibration simulations were performed on CBRW 1 to CBRW 4, with varying initial conditions. The ratio of the inertial forces ($G\dot{\theta}^2/\,I\ddot{\theta}$) of the varying amplitudes were plotted in Fig. 8. For small θ (within the relevant range of 0.05 rad or approximately five percent drift), the gyroscopic

© The 17th World Conference on Earthquake Engineering

term is not significant. However, the curved base could be designed in order to increase the gyroscopic effects as seen in CBRW 1 to CBRW 4. Moreover, if CBRWs are leveraged for other applications – e.g., tuned mass dampers – that are less constrained by drift levels, the gyroscopic effects can become more significant.

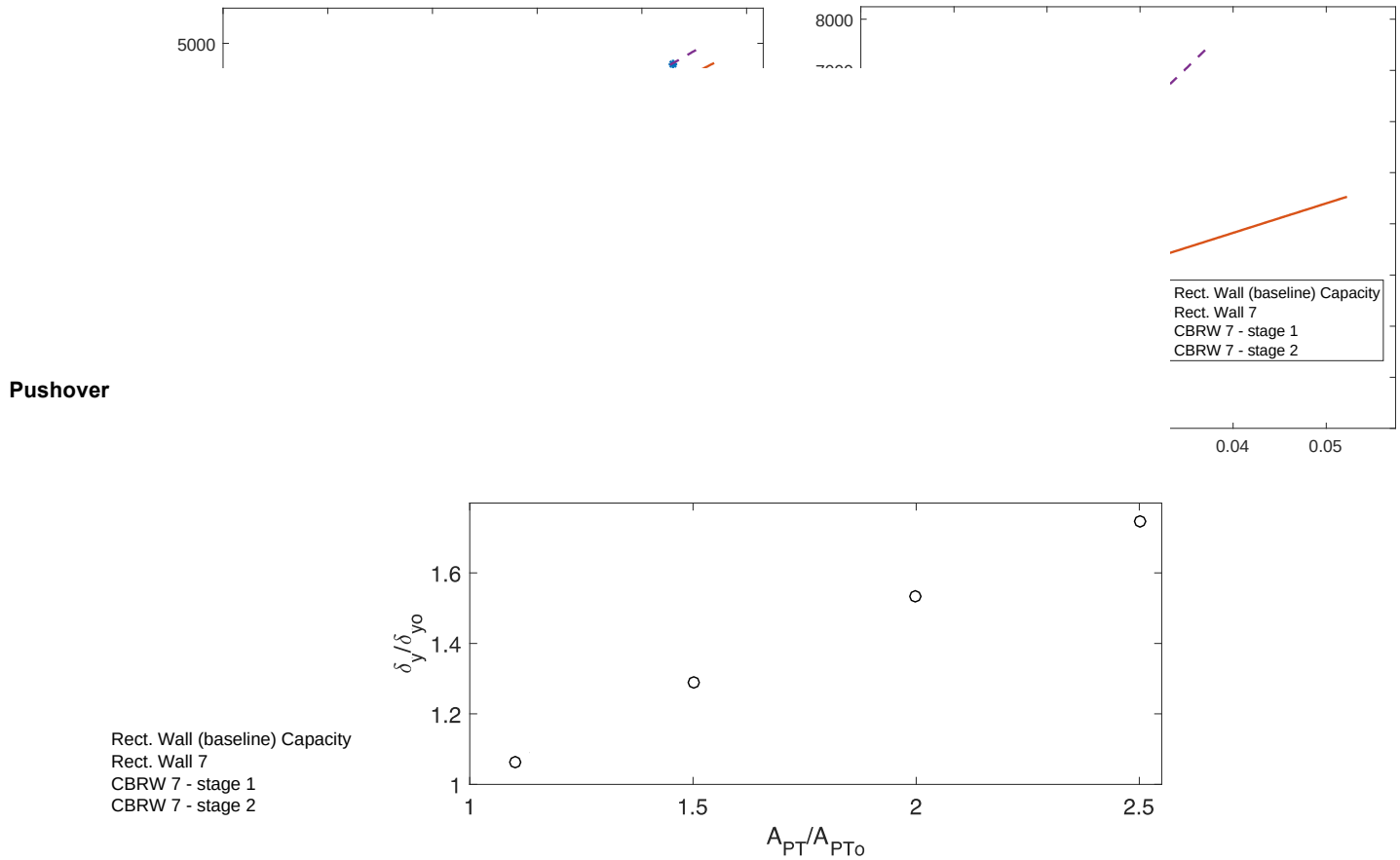

Fig. 6 – Pushover response with increasing elastic capacity: CBRW 1 (top left), CBRW 7 (top right), normalized drift at yield vs. normalized PT bar area (bottom)

5. Performance objectives of rocking walls

This section briefly discusses the performance objectives when designing rocking walls, which is more extensively discussed in [20, 26], and how it may be modified for CBRWs. The assumptions from Sec. 3.2 are no longer used herein – i.e., all real-world complexities in a rocking wall system is now considered, such as the wall flexibility and energy dissipation devices.

5.1 Performance objectives of rectangular walls

Rocking walls can be performance-based designed with four performance objectives, shown in Fig. 9 (grey curve): (1) no decompression under design wind loads, (2) no yielding in the UFP under service level earthquakes (SLE hazard level, 50% probability of exceedance in 50-year) and drift limited to 1 percent, where drift is roof drift, not interstory drift, (3) no yielding of the PT bar or crushing of the base under design basis earthquakes (DBE hazard level, 10% probability of exceedance in 50-year) and drift limited to 2 percent, and (4) no yielding of the PT bar or excessive crushing of the base under maximum considered earthquake (MCE hazard level, 2% probability of exceedance in 50-year) and drift limited to 4 percent. A review of the design process to meet these performance objectives can be found in [20, 26].

© The 17th World Conference on Earthquake Engineering

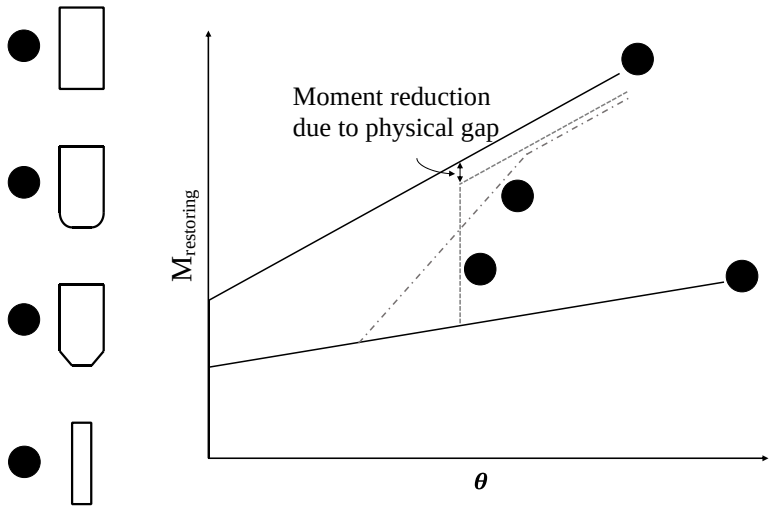

Fig. 7 – Pushover comparing rectangular and curved-base rocking walls with constant post-tensioning

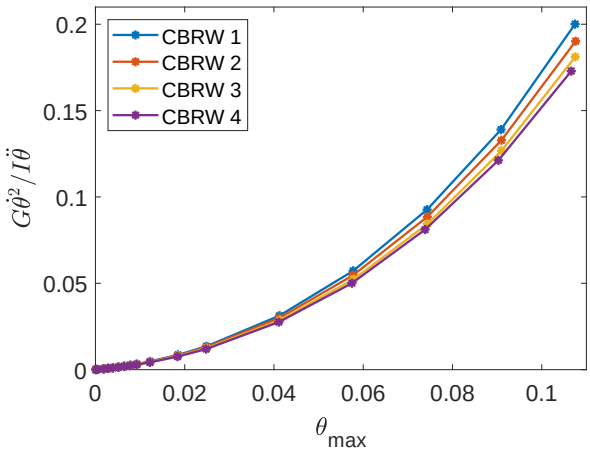

Fig. 8 – Ratio of inertial force terms vs amplitude

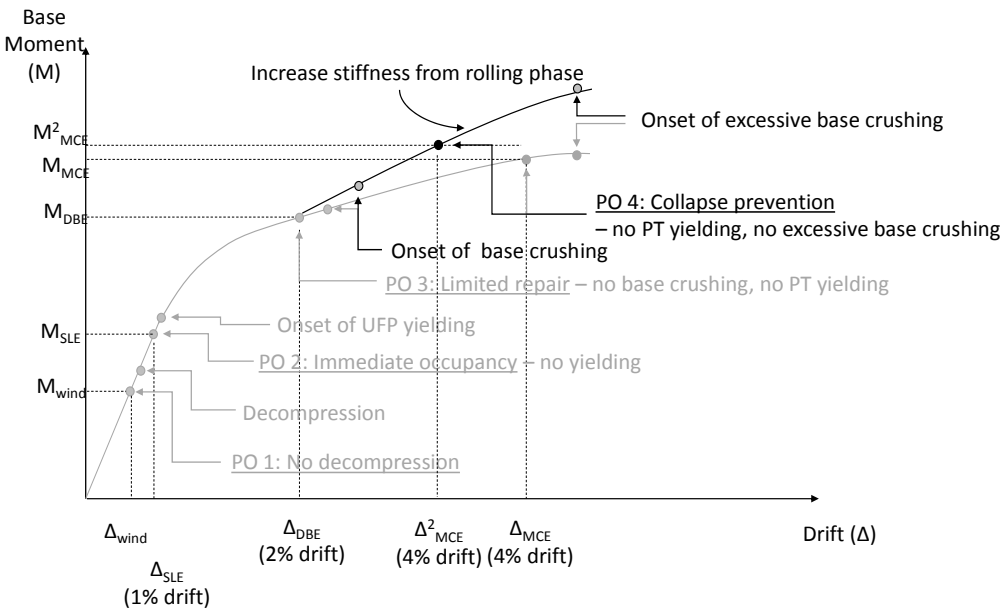

Fig. 9 – Performance objectives for post-tensioned rocking wall

© The 17th World Conference on Earthquake Engineering

5.2 Performance objectives of curved-base rocking walls

There are various additional parameters in the design space for CBRWs (h', b', and α) which would quickly result in an overwhelming number of design choices. As such, a simplified approach is presented here.

The pushover response for CBRWs are different and require further consideration on how to apply and achieve the performance objectives. From the design ideology in [28], the increase in stiffness provided by stage 2 rocking (see Sec. 5.2) is appropriate for controlling large drifts from MCE level lateral loads. Figure 9 (black curve) shows a target pushover response of a CBRW and where the performance objectives may fit. Note that this is simply an example and further work will be done to refine the performance objectives. In order to achieve these performance objectives, the design method proposed here for the CBRW is the following: (1) begin with a rectangular rocking wall; (2) design the curved base parameters such that stage 2 rocking occurs after the third performance objective but before the fourth performance objective; (3) check pushover response to ensure, prior to stage 2 rocking, it is similar to the pushover response of the rectangular wall (see Fig. 9). Though this is just one design approach, it appears most promising and tractable.

6. Conclusion

The idea of CBRWs was explored as their geometry can produce multiple lateral stiffnesses, reduce stress concentration, provide confinement to mitigate toe crushing, and increase the drift at which PT bar yielding/rupturing occurs. The analytical methodology introduced in this paper can also be used to model post-toe crushing strength/stiffness degradation in rectangular rocking walls.

The analytical equations allow for the exploration of each term of the equation of motion. It was shown that for CBRWs, a gyroscopic term, which captures the rotation-translation coupling, is in the equation of motion that is otherwise absent in rectangular walls. Additionally, the analytical equations was able to check the FE model of the CBRW. It was shown that the displacement position of the gravity frame is fairly complex for both rectangular and CBRWs for the diaphragm and wall connection used (pin and vertical slot).

Lastly, a modification to the methodology for performance-based design for rocking walls was proposed to account for the multiple rocking stages in CBRWs. Due to the large number of design parameters for CBRWs, a simple design process was presented to meet the performance objectives. Though an increase in stiffness and strength could be achieved by simply using more PT bars or a wider wall, the benefit of CBRWs is the additional tools to achieve multiple performance objectives under different seismic hazard levels.

Additional work is needed to quantify the improvements on stress concentration at the toe and to develop a design procedure that would check it is within acceptable limits. Further work is also needed to understand the effects of CBRWs on story drift and acceleration on a realistic system with energy dissipation devices excited by ground motions.

Again, this study was qualitative in nature, as the rigid wall and gravity frame assumption limits the quantitative accuracy of the analysis. In addition, the CBRW performance objectives introduced were conceptual for this preliminary study. Further work is needed to refine the design process and performance objectives. Future work will focus on modifying the CBRW model with deformable elements and contact properties that can capture material nonlinearity (especially important when looking toe crushing or concrete spalling from excessive compression).

7. References

[1] Housner G. W. (1963): The behavior of inverted pendulum structures during earthquakes. *Bulletin of the Seismological Society of America*, 1963;53:403-417.

[2] Spanos P. D., Koh A.-S. (1984): Rocking of rigid blocks due to harmonic shaking. *Journal Engineering Mechanics*, vol. 110, pp. 1627–1642.

[3] Spanos P. D., Koh A.-S. (1986): Analysis of block random rocking. *Soil Dynamics and Earthquake Engineering*, vol. 5, pp. 178–183.

© The 17th World Conference on Earthquake Engineering

[4] Yim C.-S., Chopra A. K., Penzien J. (1980): Rocking response of rigid blocks to earthquakes. *Earthquake Engineering & Structure Dynamics*, vol. 8, no. 6, pp. 565–587.

[5] Ishiyama Y. (1982): Motions of rigid bodies and criteria for overturning by earthquake excitations. *Earthquake Engineering & Structure Dynamics*, vol. 10, pp. 635–650.

[6] Koh A.-S., Spanos P. D., Roesset J. M. (1986): Harmonic rocking of rigid block on flexible foundation. *Journal Engineering Mechanics*, vol. 112, pp. 1165–1180.

[7] Aslam M., Scalise D. T., Godden W. G. (1980): Earthquake rocking response of rigid bodies. *Journal Structure Division*, vol. 106, no. 2, pp. 377–392.

[8] Hogan S. J. (1989): On the dynamics of rigid-block motion under harmonic forcing, *Proceedings of the Royal Society A: Mathematical, Physical and Engineering Sciences*, vol. 425, pp. 441–476.

[9] Bachmann J. A., Blöchlinger P., Wellauer M., Vassiliou M. F., Stojadinović B. (2016): Experimental Investigation of the seismic response of a column rocking and rolling on a concave base. *VII European Congress on Computational Methods in Applied Sciences and Engineering*, Crete Island, Greece.

[10] Christopoulos C., Filiatrault A., Folz B. (2002): Seismic response of self-centring hysteretic SDOF systems. *Earthquake Engineering & Structure Dynamics*, vol. 31, no. 5, pp. 1131–1150.

[11] Christopoulos C., Filiatrault A., Uang C.-M., Folz B. (2002): Posttensioned energy dissipating connections for moment-resisting steel frames. *Journal of Structural Engineering*, vol. 128, pp. 1111–1120.

[12] Priestley M. J. N. (1991): Overview of PRESSS research program. *PCI Journal*.

[13] Sarti F., Palermo A., Pampanin S. (2016): Quasi-static cyclic testing of two-thirds scale unbonded posttensioned rocking dissipative timber walls. *Journal of Structural Engineering*, vol. 142.

[14] Dimitrakopoulos E. G., Giouvanidis A. I. (2015): Seismic response analysis of the planar rocking frame. *Journal Engineering Mechanics*, vol. 141.

[15] Kibriya L., Ma ́laga-Chuquitaype C., Kashani M., Alexander N. (2018): Nonlinear dynamics of self-centring rocking steel frames using finite element models. *Soil Dynamics and Earthquake Engineering*, vol. 115, pp. 826–837.

[16] Alexander N., Oddbjornsson O., Taylor C., Osinga H., Kelly D. (2011): Exploring the dynamics of a class of post-tensioned, moment resisting frames. *Journal of Sound and Vibration*, vol. 330, pp. 3710–3728.

[17] Kurama Y., Pessiki S., Sause R., Lu L. W. (1999): Seismic behavior and design of unbonded post-tensioned precast concrete walls. *PCI Journal*.

[18] Henry R. S., Brooke N. J., Sritharan S., Ingham J. M. (2012): Defining concrete compressive strain in unbonded post-tensioned walls. *ACI Structure Journal*.

[19] Palermo A., Pampanin S., Buchanan A. H. (2006): Experimental investigations on LVL seismic resistant wall and frame subassemblies. *First European Conference on Earthquake Engineering and Seismology*.

[20] Ganey R. S. (2015): Seismic design and testing of rocking CLT walls. Master's thesis, University of Washington, Seattle, WA.

[21] Kramer A., Barbosa A. R., Sinha A. (2016): Performance of steel energy dissipators connected to cross-laminated timber wall panels subjected to tension and cyclic loading. *Journal of Structural Engineering*, vol. 142.

[22] Bahmani P., van de Lindt J. W., Gershfeld M., Mochizuki G. L., Pryor S. E., Rammer D. (2016): Experimental seismic behavior of a full-scale four-story soft-story wood- frame building with retrofits. I: Building design, retrofit methodology, and numerical validation. *Journal of Structural Engineering*, vol. 142.

[23] van de Lindt J. W., Bahmani P., Mochizuki G., Pryor S. E., Gershfeld M., Tian J., Symans M. D., Rammer D. (2016): Experimental seismic behavior of a full-scale four- story soft-story wood-frame building with retrofits. II: Shake table test results. *Journal of Structural Engineering*, vol. 142.

[24] Eatherton M. R., Ma X., Krawinkler H., Mar D., Billington S., Hajjar J. F., Deierlein G. G. (2014): Design concepts for controlled rocking of self-centering steel-braced frames, *Journal of Structural Engineering*, vol. 140.

[25] Pampanin S., Priestley M. J. N., Sritharan S. (2001): Analytical modelling of the seismic behaviour of precast concrete frames designed with ductile connections. *Journal of Earthquake Engineering*, vol. 5, pp. 329–367.

© The 17th World Conference on Earthquake Engineering

[26] Wichman S. (2018): Large-scale dynamic testing of rocking cross laminated timber walls. Master's thesis, University of Washington

[27] McKenna F. (1997): Object-oriented finite element programming: Frameworks for analysis, algorithms and parallel computing. PhD thesis, University of California, Berkeley.

[28] Kelly J. M. (1999): The role of damping in seismic isolation. *Earthquake Engineering & Structural Dynamics*, vol. 28, pp. 3–20.

© The 17th World Conference on Earthquake Engineering